Nanoscale

PAPER

View Article Online
View Journal | View Issue

Cite this: *Nanoscale*, 2020, **12**, 24169

Thermal properties of lipid bilayers derived from the transient heating regime of upconverting nanoparticles†

Ana R. N. Bastos, [a] Carlos D. S. Brites, [a] Paola A. Rojas-Gutierrez, [b] Rute A. S. Ferreira, [a] Ricardo L. Longo, *[c] Christine DeWolf, [b] John A. Capobianco *[b] and Luís D. Carlos *[a]

Received 29th September 2020,
Accepted 24th November 2020

DOI: 10.1039/d0nr06989b

rsc.li/nanoscale

Heat transfer and thermal properties at the nanoscale can be challenging to obtain experimentally. These are potentially relevant for understanding thermoregulation in cells. Experimental data from the transient heating regime in conjunction with a model based on the energy conservation enable the determination of the specific heat capacities for all components of a nanoconstruct, namely an upconverting nanoparticle and its conformal lipid bilayer coating. This approach benefits from a very simple, cost-effective and non-invasive optical setup to measure the thermal parameters at the nanoscale. The time-dependent model developed herein lays the foundation to describe the dynamics of heat transfer at the nanoscale and were used to understand the heat dissipation by lipid bilayers.

Introduction

During metabolism cells undergo continuous heat transfer. However, very little is known about the heat transfer at the cellular level, and in particular about the thermal properties of each of the cellular components.[1–5] Frequently the thermal conductivity and/or heat transfer coefficients of the lipid membrane, proteins, and intracellular fluid are all assumed to be the same, an inaccuracy highlighted by Suzuki and Plakhotnik.[5] The thermal properties of the cell membrane itself are important in thermoregulation, *i.e.* the heat transfer from the cell to the surrounding environment and *vice versa*. The cell membrane is best approximated by a phospholipid bilayer that has been employed extensively for investigating the membrane thermodynamic and thermal properties both experimentally[6,7] and computationally.[8–10] While much of the phospholipid literature is focused on the thermotropic phase behaviour, absolute measurements of intrinsic lipid bilayer thermodynamic properties are less accessible.

Luminescent nanothermometry[11–15] has been widely used in the determination of cell temperature, which relies on luminescent probes such as proteins, dyes, fluorescent gold nanoclusters and nanoparticles.[5,16–19] Furthermore, the technique has been recently used to measure the core temperature of upconverting nanoparticles (UCNPs) coated with a lipid bilayer enabling the direct determination of the thermal conductivity of the coating, with advantages relative to the established experimental electrical methods.[20] However, simply measuring the temperature, a state variable, does not provide an insight into the dissipation of heat which is dynamic thus, requiring that the transient regime be studied.

Herein, we employ a nanoconstruct comprising a UCNP ($LiYF_4$:Er^{3+}/Yb^{3+}) surrounded by a conformal supported lipid bilayer (containing dioleoylphosphatidylcholine, DOPC, dioleoylphosphatidic acid, DOPA, cholesterol, and oleate)[20,21] to develop a model and demonstrate experimentally that the transient regime permits to obtain the specific heat capacity of both the lipid bilayer and the UCNP. In contrast, the steady-state regime only yields an estimate of the conduction heat transfer of both components of the nanoconstruct. The determination of the specific heat capacity at the nanoscale is challenging, less explored and important to clarify why nanofluids show enhanced specific heat capacities. This property has been observed upon the addition of nanoparticles to a molten

[a]*Phantom-g, CICECO – Aveiro Institute of Materials, Department of Physics, University of Aveiro, 3810-193 Aveiro, Portugal. E-mail: lcarlos@ua.pt*
[b]*Department of Chemistry and Biochemistry, and Centre for NanoScience Research, Concordia University, 7141 Sherbrooke St. West, Montreal, Quebec, H4B 1R6, Canada. E-mail: John.Capobianco@concordia.ca*
[c]*Departamento de Química Fundamental, Universidade Federal de Pernambuco, Cidade Universitária, 50740-560 Recife, PE, Brazil. E-mail: ricardo.longo@ufpe.br*
†Electronic supplementary information (ESI) available. See DOI: 10.1039/d0nr06989b

salt, that has technological relevance in energy storage, however, the mechanism is not yet understood.[22]

Experimental details

Materials

Dispersions of tetragonal phase $LiYF_4$:Er^{3+}/Yb^{3+} were synthesized *via* thermal decomposition. Capped UCNPs have been coated with a conformal supported lipid bilayer coating. The capped and uncapped (oleate-free[23]) nanoparticles are dispersed in either ultrapure H_2O or D_2O (dispersion concentrations are based on the dry weight of nanoparticles). Nanoparticles were characterized using transmission and scanning electron microscopy and X-ray diffraction. Properties of the UCNPs are provided in section I of the ESI and in Tables S1 and S2.† Details of the synthesis and characterization of the nanoparticles have been reported previously.[21]

Methods

Dynamic temperature measurements. The temperature increase (ΔT) when the nanofluids are under NIR irradiation at 980 nm depends on the laser power density (P_D) and on the composition of the nanofluid (presence or absence of a conformal lipid bilayer and the solvent used, as previously observed[20]), section II of the ESI.† The nanofluids were irradiated for 600 s by a pulsed laser (BrixX 980-1000 HD, 1.5 MHz) at 980 nm, with power densities ranging from *ca.* 65 to 250 W cm^{-2} (as described in section III of the ESI†). The resulting temperature increase was measured over time using an immersed thermocouple (K-type, 0.1 K accuracy) placed *ca.* 0.5 cm away from the limits of the laser spot and always at the same place along the optical pathlength (Fig. 1). Because the size of the thermocouple is small (*ca.* 1.5 mm), there is little variation (<4%) of ΔT along the excitation cylinder of the laser beam path. In addition, it can be shown (sections IV–VI of the ESI†) that the temperature variation across the laser beam is negligible ($\lesssim$0.06 K) because its diameter is very small. This was estimated by using a very narrow profile and can be considered as an upper bound for the temperature variation. Therefore, accounting for the observed Gaussian profile of the laser beam would yield an even smaller temperature variation. As a result, the temperature increase, $\Delta T(t)$, monitored by the thermocouple can be considered uniform (section VI of the ESI†). During the measurements, the thermocouple was kept at a fixed distance from the laser beam to avoid changes in the transient regime profile.

It is relevant to determine how ΔT, associated with absorption, varies across and along the excitation cylinder of the laser beam path, which will determine the accuracy and reliability of the derived properties as well as establish the temperature monitoring. Assuming constant thermal conductivity, and that the power absorbed from the laser beam is converted into heat, the temperature variation across the laser beam path is $T_{surface} - T_{centre} = (N_{P,b}\sigma_P + \sigma_S)P_D/4\pi\kappa L$, which under the experimental conditions used corresponds to a

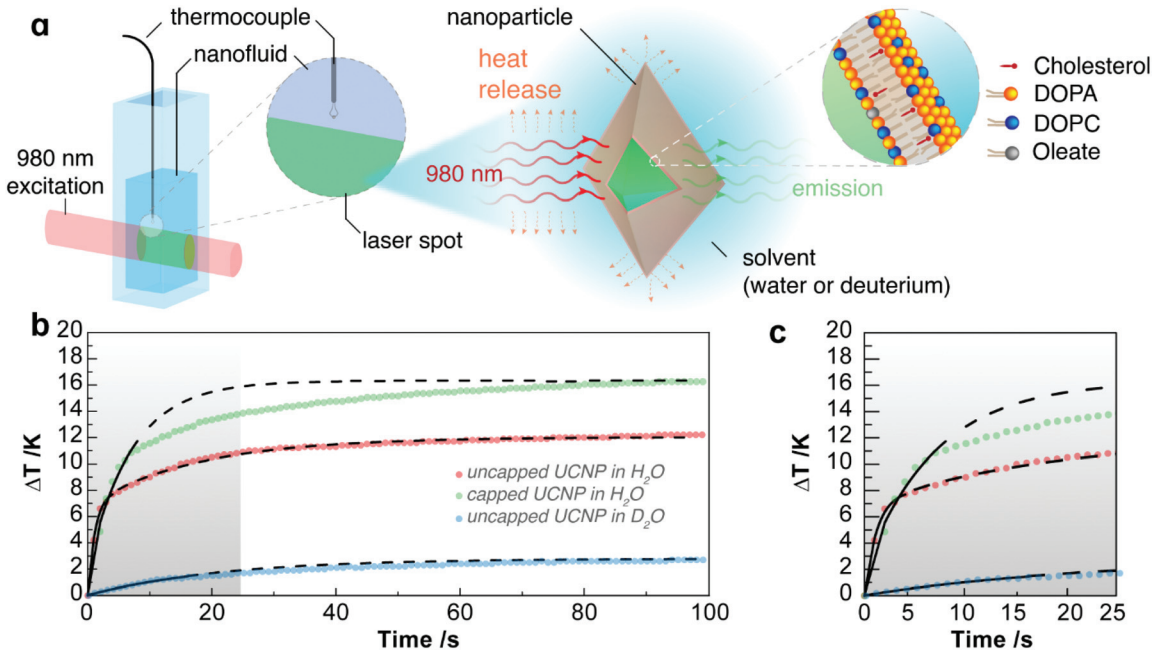

Fig. 1 (a) Schematic of the experimental setup used to record the temporal dependence of the temperature of the nanofluids under 980 nm excitation. The magnification of the laser spot on the nanofluid represents the heat exchange between the solvent (H_2O or D_2O) and the nanoparticle due to 980 nm excitation, and the composition of the conformal lipid bilayer coating the surface of the nanoparticle. (b) Temperature profiles of the uncapped UCNPs and lipid bilayer-capped UCNPs dispersed in H_2O, and uncapped UCNPs dispersed in D_2O, measured under 980 nm excitation (222 W cm^{-2}) using the immersed thermocouple. Dashed lines are fits for the entire data set and continuous lines are fits of the initial period of NIR irradiation. (c) Magnification of the first 25 s (shaded area of (b)) highlighting the fit of the model in the initial period of 980 nm irradiation.

temperature variation of 0.061 K. Given the small size of the focal point, ΔT can be assumed to be spatially homogenous within this region (section VI of the ESI†). Regarding the temperature variation along a cylinder defined by the path of the laser beam, the exponential attenuation of the radiant power of the laser beam causes a monotonic decrease of ΔT along the optical pathlength by *ca.* 1.6 times (section VI of the ESI†). Therefore, it is very important to ensure that the temperature is always monitored in the same position. Note that temperature monitoring by ratiometric luminescence using the UCNPs will not be addressed here.

Description of the fitting procedure. The experimental data were fit to a first-order exponential decay function. The fit was limited to the first regime of each transient curve, which was established through the linearized representation of the data (Fig. 2). For each sample, a multi-fit was performed in which all of the transient curves were fitted simultaneously to eqn (16). As ΔT_{ss} depends on the laser power density, it was fixed for each curve and constrained by the respective errors. In the multi-fit, the parameter τ was set as a free variable and identical for all the curves enabling the determination of the c_p and c_L values.

Upconversion quantum yield. Absolute upconversion quantum yield values were measured in the Quantaurus-QY (C13534, Hamamatsu) system equipped with an integrating sphere as sample chamber and two multi-channel analyzers for signal detection in the visible and the NIR spectral ranges. A 980 nm external laser diode (FC-980 5 W, CNI Lasers) was used as the excitation source. Since the emission quantum yield of UCNPs depends on the excitation power density,[24–26] the comparison of the performance of upconverting phosphors should be made using the saturation regime, corresponding to the maximum emission quantum yield value.[27] Here, P_D = 950 W cm^{-2} (considering the illumination area in the sample holder, 0.0025 cm^2, according to the manufacturer) in the saturation regime. The measurements were done in quartz cuvettes of 1 cm optical path, filled with 2 mL of UCNPs at 0.6 g L^{-1} concentration. As a reference sample, the empty cuvette was used. Three measurements were made and the mean value is reported. According to the manufacturer, the measurements present a relative error of 10%.

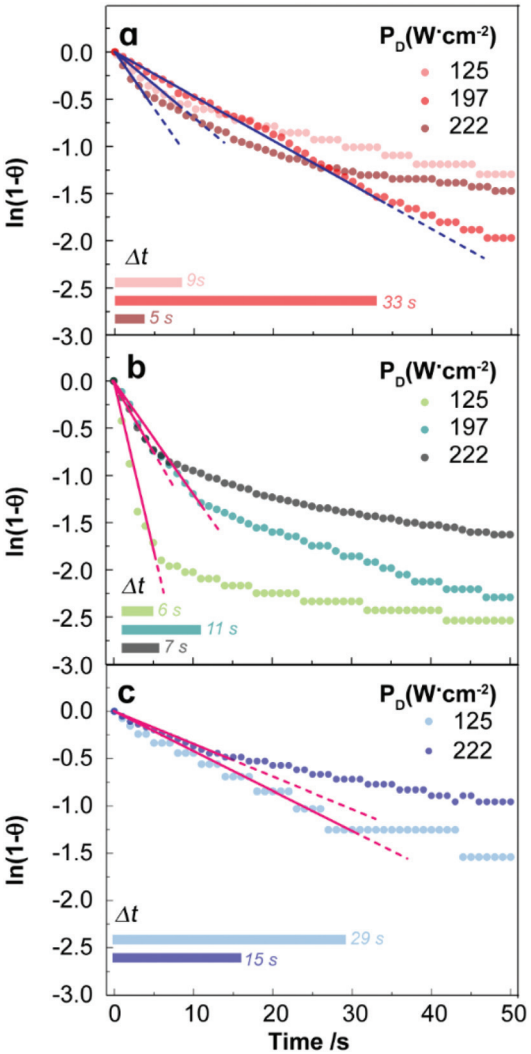

Fig. 2 Time-dependence of the reduced temperature for the (a) uncapped UCNPs and (b) lipid bilayer-capped UCNPs dispersed in H_2O, and (c) uncapped UCNPs dispersed in D_2O, measured by the immersed thermocouple. The logarithmic representation of the reduced temperature profiles allows the identification of the time range in which ln[1 – $\theta(t)$] is linear. The horizontal bars mark the time interval (Δt) in which these linear fits are verified. The solid lines are the best fits to eqn (16) (r^2 > 0.970) and the dashed lines are guides for the eyes.

Results and discussion

Laser heating of nanofluids containing upconversion nanoparticles, UCNPs, including capped-UCNPs, has been performed, and by analyzing the temperature increase at steady-state, the thermal conductivities of the nanofluids were determined.[20,21] However, for analysis of the transient regime, a time-dependent approach is necessary and additional considerations are in order.

Modelling laser heating of nanofluids: power balance

As a laser beam travels through a nanofluid, photons are absorbed by the medium and this absorbed energy is converted into heat, which will cause an increase of temperature. Under the experimental conditions, the optical pathlength is *ca.* 100 times larger than the diameter of the laser spot, so the laser beam can be considered as a long cylinder and the heat will be dissipated radially from the surface of this cylinder. As a result, the heat dissipation along the laser path is negligible and considering that only the particles within this cylinder will absorb and cause heating, the process can be described by a one-dimensional (radial) heat transfer with cylindrical symmetry. To model this heating process, each of the components of the nanofluid (UCNPs, lipid bilayer and solvent) will be considered as independent. The total absorption cross-section will then be the sum of the absorption cross-sections of the indi-

vidual components. This applies similarly to the heat transfer properties of the nanofluid, particularly, heat capacity.

The time at which the irradiation starts (the initial time) is denoted by t_0. The temperature, $T(t)$, increases up to a constant value, the so-called steady-state regime, $T(t_{ss}) \equiv T_{ss}$. The period during which the temperature increases from the initial equilibrium temperature of the sample, $T(t_0) \equiv T_0$, to its steady-state value, T_{ss}, denoted by $\Delta t = t_{ss} - t_0$, defines the transient regime.

Energy conservation dictates that, on average, the total energy of an isolated system is constant, *i.e.* it is conserved over time. Thus, the power (or energy rate) gained, W_{gain}, has to be equal the power lost (or dissipated), W_{lost}:

$$W_{gain} = W_{lost} \quad (1)$$

This is the power balance equation, which can be obtained from the transient heat transfer differential equation derived using, for example, the shell balance approach[28] under homogeneous conditions of the thermal conductivity and of the temperature gradient. The power balance equation has been successfully applied to several nanosystems, particularly in describing processes such as laser-induced incandescence.[29,30] The simplicity to setup and to solve this equation is one of its appeals because only the processes of power gains and power losses associated with the experimental conditions are required. In the case of laser heating of nanofluids, the power gain is basically that absorbed from the laser beam, so that $W_{gain} = W_{abs}$, where the rate of energy absorption, W_{abs}, can be determined as (section IV of the ESI†)

$$W_{abs} \cong (N_{P,b}\sigma_P + N_{P,b}\sigma_L + \sigma_{S,b})P_D \quad (2)$$

where $N_{P,b}$ is the number of nanoparticles (dimensionless) exposed to the laser beam, σ_P (in m^2) is the absorption cross-section of a single nanoparticle, σ_L (in m^2) is the absorption cross-section of the lipid bilayer coating, $\sigma_{S,b}$ (in m^2) is the absorption cross-section of the solvent within the path of the laser beam, and P_D (in W m^{-2}) is the incident power density. The absorption cross-sections were determined from the absorption spectra of the nanofluids and the number density of each species was calculated from its concentration in solution and its mass or from its molar mass and density for a pure substance. The power dissipation has several pathways and mechanisms that need to be identified, quantified, and evaluated.

Power lost or dissipated

The main mechanisms and pathways of energy dissipation are: (i) heat transfer *via* conduction, convection, and thermal radiation, (ii) increase of internal energy due to heat capacity, and (iii) upconversion emission by the UCNPs. Other sources of heat dissipation such as evaporation, ionization, dissociation, *etc*. will not be considered because of the stability of the systems and the relatively small temperature increase. In addition, the effects of the coupling between the flow of heat and the flow of matter, *e.g.* the Soret (or thermophoresis, or thermal diffusion) and the Dufour (heat flow caused by a concentration gradient) effects will not be considered. Derivations and calculations of the main contributions to heat dissipation are presented in section V of the ESI.†

Power dissipation *via* heat transfer

The heating of the nanofluid within the path of the laser beam creates a temperature gradient between the excitation cylinder and the bulk of the sample that is at room temperature. So, the temperature varies radially from $T(t)$ at the surface of the cylinder to T_0. According to Fourier's law of heat conduction,[31] the rate of heat dissipation by conduction, W_{cond} (in W), is proportional to the temperature gradient. Given the spatial homogeneity of the system and the small temperature increase caused by the laser heating, the temperature gradient can be approximated by its finite difference form as

$$\begin{aligned} W_{cond}(t) &= A_{cs}\kappa_m \frac{\partial T(r,t)}{\partial r} \cong A_{cs}\kappa_m \frac{\Delta T(t)}{\Delta r} \\ &= A_{cs}h_{cond}\Delta T(t), \quad h_{cond} = \frac{\kappa_m}{\Delta r} \end{aligned} \quad (3)$$

where A_{cs} (in m^2) is the cross-sectional area of the heat flux, κ_m (in W m^{-1} K^{-1}) is the thermal conductivity of the medium, h_{cond} (in W m^{-2} K^{-1}) is the thermal conduction coefficient, and Δr is a radial distance over which the temperature decreases from $T(t)$ to room temperature T_0. Notice that this typical radial distance, Δr, relates the thermal conduction coefficient, h_{cond}, with the thermal conductivity, κ_m.

A hotter region can also dissipate heat to a colder region *via* convection. So, according to Newton's cooling law the convective heat dissipation, $W_{conv}(t)$,[31] by the laser heated nanofluid is

$$W_{conv}(t) = A_{cs}h_{conv}\Delta T(t) \quad (4)$$

where h_{conv} (in W m^{-2} K^{-1}) is the convection heat transfer coefficient. In general, the convection process can be classified as free, forced, and phase change (*e.g.* boiling or condensation).

Matter at a temperature above 0 K emits thermal radiation with an upper limit to its emissive power given by the Stefan–Boltzmann law, which is proportional to the fourth power of the temperature. It also absorbs thermal radiation from the environment, which is governed by the same law. However, when the body is at a temperature $T(t)$ higher than its surroundings T_0, a net power dissipation, $W_{rad}(t)$, will be established due to thermal radiation, which can be expressed as[31]

$$W_{rad}(t) = \varepsilon\sigma_{SB}A_{cs}[T^4(t) - {T_0}^4] = A_{cs}h_{rad}\Delta T(t) \quad (5)$$

where $0 \leq \varepsilon \leq 1$ is the emissivity of the heated region and σ_{SB} (in W m^{-2} K^{-4}) is the Stefan–Boltzmann constant. The last equality in eqn (5) is obtained when the thermal radiation coefficient, h_{rad} (in W m^{-2} K^{-1}), is defined as

$$h_{rad} = \varepsilon\sigma_{SB}[T(t) + T_0][T^2(t) + {T_0}^2] \quad (6)$$

It is noteworthy that all three contributions to the power dissipation *via* heat transfer, namely, the approximated expression in eqn (3) for conduction, eqn (4) for convection,

and eqn (5) for thermal radiation have the same functional form, so they can be combined into

$$W_{\mathrm{ht}}(t) = h_{\mathrm{ht}} A_{\mathrm{cs}} \Delta T(t) \tag{7}$$

where W_{ht} is the power loss due to heat transfer and h_{ht} (in W $\mathrm{m^{-2}\ K^{-1}}$) is the heat transfer coefficient, which is a sum of the conduction, convection and thermal radiation coefficients. Given the experimental conditions, one of these coefficients might dominate and thus determine the main mechanism of heat transfer.

Power loss *via* upconversion emission

The UCNPs in the nanofluid absorb radiation from the near-infrared laser and emit radiation in the visible region. This process will then decrease the amount of absorbed energy that is transformed into heat, so it will not contribute to the heating of the nanofluid and can be considered as dissipated power. From the definition of the quantum yield and the energies of the absorbed and emitted photons during the upconversion (UC) process, the power loss due to upconversion emission, W_{UC}, can be expressed as

$$W_{\mathrm{UC}} = \frac{\tilde{\nu}_{\mathrm{em}}}{\tilde{\nu}_{\mathrm{abs}}} \phi_{\mathrm{UC}} N_{\mathrm{P,b}} \sigma_{\mathrm{P}} P_{\mathrm{D}} \sim 10^{-5} N_{\mathrm{P,b}} \sigma_{\mathrm{P}} P_{\mathrm{D}} \tag{8}$$

where $\tilde{\nu}_{\mathrm{abs}}$ and $\tilde{\nu}_{\mathrm{em}}$ are the absorption and emission wavenumbers, ϕ_{UC} is the quantum yield of the upconversion process, $N_{\mathrm{P,b}}$ is the number of UCNPs within the path of the laser beam, σ_{P} is the absorption cross-section of a single UCNP, and P_{D} is the power density of the incident laser beam. The ϕ_{UC} values for the uncapped and lipid bilayer-capped $LiYF_4$:Er^{3+}/Yb^{3+} UCNPs dispersed in water were measured as $(0.040 \pm 0.004) \times 10^{-4}$ and $(0.120 \pm 0.010) \times 10^{-4}$, respectively, justifying the last approximation in eqn (8) ($\tilde{\nu}_{\mathrm{em}}/\tilde{\nu}_{\mathrm{abs}} \cong 0.5$). As far as we know, this is the first report of absolute emission quantum yields in $LiYF_4$:Er^{3+}/Yb^{3+} UCNPs. The values obtained here are of the same order of magnitude as those recorded for SrF_2:Er^{3+}/Yb^{3+} UCNPs,[26] although smaller than those reported for $LiYF_4$:Tm^{3+}/Yb^{3+} UCNPs dispersed in toluene and $NaYF_4$:Er^{3+}/Yb^{3+} UCNPs suspended in water.[24,32] However, we note that the use of different solvents, hosts, dopant ions, dopant concentrations, and particle sizes preclude the direct comparison between values.

Notice that power loss *via* emission at *ca.* 980 nm by Yb^{3+} and in the NIR region by Er^{3+} were not considered because the energy transfer upconversion rates from excited Yb^{3+} to Er^{3+} are much larger than the radiative decay of excited Yb^{3+}.[33–35] Consequently, emissions in the NIR region are not observed, as shown in Fig. S5 (section IX of the ESI†).

Power loss *via* the increase of internal energy

Because the nanofluid within and surrounding the excitation cylinder of the laser beam has a heat capacity, c_{N}, it can store energy and the rate of energy storage or the rate of internal energy increase, $W_{\mathrm{int}}(t)$, is

$$W_{\mathrm{int}}(t) = m_{\mathrm{N}} c_{\mathrm{N}} \frac{\mathrm{d}T(t)}{\mathrm{d}t} \tag{9}$$

where m_{N} (in kg) is the mass of the nanofluid and c_{N} (in $\mathrm{J\ K^{-1}\ kg^{-1}}$) is the heat capacity of the region where the temperature is increasing. As it was assumed that the species constituting the nanofluid are independent, its capacity to store heat can be separated into two contributions

$$m_{\mathrm{N}} c_{\mathrm{N}} = m_{\mathrm{P}} c_{\mathrm{P}} + m_{\mathrm{S}} c_{\mathrm{S}} \tag{10}$$

with m_{P} and c_{P} being the mass and heat capacity of the nanoparticles, m_{S} and c_{S} the mass and heat capacity of the solvent. Furthermore, when the nanoparticles are capped by a lipid bilayer, then

$$m_{\mathrm{N}} c_{\mathrm{N}} = m_{\mathrm{P}} c_{\mathrm{P}} + m_{\mathrm{S}} c_{\mathrm{S}} + m_{\mathrm{L}} c_{\mathrm{L}} \tag{11}$$

where m_{L} and c_{L} are the mass and heat capacity of the lipid bilayer.

Power balance equation and analysis

The power dissipated from the laser heated nanofluid can then be approximated by the sum of contributions in eqn (7), (8), and (9), that is, $W_{\mathrm{lost}} \cong W_{\mathrm{ht}}(t) + W_{\mathrm{UC}} + W_{\mathrm{int}}(t)$. Considering that the power gain for the laser heating of the nanofluid is due to absorption from the laser beam: $W_{\mathrm{gain}} = W_{\mathrm{abs}}$, which is assumed to be completely converted into heat, the following expression for the power balance, eqn (1), can be obtained

$$W_{\mathrm{abs}} = h_{\mathrm{ht}} A_{\mathrm{cs}} \Delta T(t) + W_{\mathrm{UC}} + m_{\mathrm{N}} c_{\mathrm{N}} \frac{\mathrm{d}\Delta T(t)}{\mathrm{d}t} \tag{12}$$

where $\Delta T(t) = T(t) - T_0$, so $\mathrm{d}\Delta T(t)/\mathrm{d}t = \mathrm{d}T(t)/\mathrm{d}t$. This equation has the following solution

$$\begin{aligned} \Delta T(t) &= \Delta T_{\mathrm{ss}} \left(1 - e^{-\frac{t}{\tau}}\right) \\ \frac{1}{\tau} &= \frac{W_{\mathrm{abs}} - W_{\mathrm{UC}}}{m_{\mathrm{N}} c_{\mathrm{N}} \Delta T_{\mathrm{ss}}} \cong \frac{W_{\mathrm{abs}}}{m_{\mathrm{N}} c_{\mathrm{N}} \Delta T_{\mathrm{ss}}} \end{aligned} \tag{13}$$

for the initial condition: $\Delta T(t) = 0$, with W_{abs} being the power absorbed from the laser beam.

An interesting feature of the model quantified in eqn (13) is that the measurement of the temperature increase $\Delta T(t)$ could be performed by luminescence thermometry with the UCNPs and/or with a thermocouple. These measurements should yield different temperatures because of their distinct locations within the nanofluid. However, it is expected that both measurements would provide the same temperature profile during the transient regime because the medium between the laser beam and the thermocouple is constant. To ensure this latter statement, the thermocouple should be always placed at the same position relative to the laser beam. In the present experimental setup, the excitation of the UCNPs will depend on their positions along the optical path, so a direct temperature measurement from the luminescence is not viable and further modeling or a different experimental setup is required. Hence, the increase $\Delta T(t)$ during the transient regime was determined only by a thermocouple with a narrow area.

It is evident from eqn (8), that the power dissipated by the upconversion process, W_{UC}, is smaller than *ca.* 0.05% of the power absorbed by the UCNPs within the laser beam. As a

result, the ratio W_{UC}/W_{abs} is smaller than 10^{-5} (section V of the ESI†), which justifies the approximation in eqn (13).

The solution of the equation describing the laser heating of a nanofluid also provides the following expression for the increase of temperature at the steady-state regime

$$\Delta T_{ss} \cong \frac{W_{abs}}{h_{ht} A_{cs}}, \qquad W_{abs} = (N_{P,b}\sigma_P + N_{P,b}\sigma_L + \sigma_S) + P_D \tag{14}$$

where the approximation $W_{abs} - W_{UC} \cong W_{abs}$ was used. Considering the sample temperature T_0 = 300 K and a temperature increase ΔT = 10 K, the flux of heat dissipation *via* thermal radiation, W_{rad}/A_{cs}, is negligible (100 times smaller) compared to the flux of heat dissipation *via* conduction, W_{cond}/A_{cs}, for a dilute aqueous dispersion. Since the dispersions are not stirred during the laser heating process, the heat transfer *via* convection may be considered negligible, so that conduction becomes the main mechanism of heat transfer and $h_{ht} \cong h_{cond}$. Therefore, analysis of the steady-state regime yields eqn (14), which is consistent with previous work that reported this property the thermal conductivity properties of luminescent and composite nanofluids.[20]

It is noteworthy that the transient regime described by eqn (13) does not require the determination of the heat transfer properties of the nanofluids, as long as ΔT_{ss} is considered a parameter that can be determined experimentally. In other words, the transient regime is fully described by ΔT_{ss} and τ which can be related to the heat transfer properties and the heat capacities of nanofluids, respectively. In fact, the heat capacity, c_N, of the nanofluid can be obtained as

$$c_N = \frac{W_{abs}\tau}{\Delta T_{ss} m_N}, \qquad W_{abs} = \sigma_N P_D = \left(N_{P,b}\sigma_P + N_{P,b}\sigma_L + \sigma_S\right)P_D \tag{15}$$

where, as mentioned before, the power absorbed, W_{abs}, can be determined from the laser power density, P_D, and the absorption cross-section of the nanofluid, $\sigma_N = N_{P,b}\sigma_P + N_{P,b}\sigma_L + \sigma_S$. The temperature increase at steady-state, ΔT_{ss}, can be measured for each laser power density employed,[20] whereas τ can be obtained from the fitting of the temperature increase during the transient regime. Regarding the determination of τ, it is relevant to notice that the $\Delta T(t)$ *vs.* t data are dominated by the steady-state regime, as shown in Fig. 1b, c and Fig. S2a.†

Thus, a direct fit of eqn (13) is not appropriate and the following linearized form using the reduced temperature, $\theta(t)$, was employed where τ was obtained from the inverse of the slope of the linear regime (Fig. 2 and Fig. S2b†).

$$\ln[1 - \theta(t)] = -\frac{1}{\tau}t, \quad \theta(t) \equiv \frac{\Delta T(t)}{\Delta T_{ss}} \tag{16}$$

As shown in Fig. 2 and Fig. S2b,† the transient regime is accurately described by the linearized model which enables the establishment of the limits of the first regime of the transient curve. This analysis was applied to samples of pure water, and dispersions of uncapped and capped UCNPs in H_2O and D_2O for several laser power densities. An example of the transient properties is shown in Table 1. The complete data related to these properties are presented in the ESI (Tables S6–S8†).

Table 1 Properties of nanofluids derived from laser heating for a power density of 222 W cm^{-2}

Fluid	W_{abs} (mW)	ΔT_{ss} (K)	τ (s)
Pure water	8.93 ± 0.83	8.2 ± 0.1	0.31 ± 0.01
UCNPs in H_2O	9.03 ± 0.72	13.8 ± 0.1	0.51 ± 0.03
Capped-UCNPs in H_2O	9.08 ± 0.92	16.2 ± 0.1	0.60 ± 0.03
UCNPs in D_2O	0.35 ± 0.24	3.9 ± 0.1	4.21 ± 0.39

As expected from the absorption spectra of the fluids, the absorbed power, W_{abs}, is dominated by H_2O, and even for D_2O its contribution is significant. The lipid bilayer also has a significant impact on the optical properties of the UCNPs. In fact, the lipid bilayer doubles the absorption cross-section of the UCNPs, from 0.16 to 0.32 nm^2, despite the small increase of *ca.* 14% of the geometrical cross-section, from 2255 nm^2 for the uncapped UCNP to 2570 nm^2 for the capped UCNP. This significant increase of the absorption cross-section at 980 nm is due to the presence of high energy oscillators such as O–H, N–H, and C–H associated with the lipid bilayer and with hydration molecules in the nanoconstruct (supported lipid bilayer-coated UCNPs). However, despite W_{abs} being dominated by water, the nanoparticles have a significant effect on the thermal properties of the fluid, causing a steep increase of ΔT_{ss} and τ.

Analysis of the transient regime at three power densities for water (Fig. S4 and Table SI†) yielded a heat capacity of 4177 ± 367 J kg^{-1} K^{-1}, which agrees within the uncertainty with the reported value of 4181 ± 4 J kg^{-1} K^{-1} at 298 K,[36] showing the reliability of the proposed approach. For the nanofluid comprising uncapped UCNPs in H_2O, the heat capacity of water shown above was subtracted and a value of 715 ± 57 J kg^{-1} K^{-1} for the uncapped UCNPs was obtained. This value is in reasonable agreement with that reported for $LiYF_4$ crystals at room temperature (790 J kg^{-1} K^{-1}).[37–39] Despite the instability of the suspension of UCNPs dispersed in D_2O, a value for the heat capacity of uncapped UCNPs of 709 ± 93 J kg^{-1} K^{-1} could be derived from measurements at two laser power densities which is also in agreement with the reported value for $LiYF_4$ crystals. Through this analysis, the main sources of the uncertainty of the heat capacity are the quantities appearing in eqn (15), namely: (i) mass of the UCNPs; (ii) number of species exposed to the laser beam; (iii) absorption cross-sections; (iv) power density and (v) measured parameters τ and ΔT_{ss}. Note that this analysis also considers the specific heat capacity to be independent of temperature. Nonetheless, because the temperature increase over the transient regime is at most *ca.* 10 K (Fig. 1c and Fig. S4†), this limitation causes a small relative uncertainty of *ca.* 0.03% and 3% in the final values for water and the uncapped UCNPs, respectively.

Table 2 Comparison of the heat capacity values of lipid bilayers, c_L, obtained using different techniques

Compound	c_L ($J\ kg^{-1}\ K^{-1}$)	c_L ($kJ\ mol^{-1}\ K^{-1}$)	Technique	Ref.
Oleate : DOPA : DOPC : cholesterol (21 : 51 : 5 : 24)	5039 ± 211	2.93 ± 0.12	Transient heating of nanofluids	This work
DPPC	3678	2.7	Atomistic molecular dynamics simulations	44
DPPC	2166	1.59	Differential scanning calorimetry[b]	45
DPPE[a]	2268	1.57		

[a] DPPE: dipalmitoylphosphatidylethanolamine. [b] Measured at 293 K.

To the best of our knowledge, this is the first time that the heat capacity of a UCNP has been measured. The similarity of the heat capacity of the UCNPs to that of the bulk $LiYF_4$ may be attributed to the size of the nanoparticles employed (Table S2†). Specifically, although the literature provides very little data (experimental and computational) for the heat capacities of nanomaterials, it has been reported that particles with sizes larger than *ca.* 70 nm have thermal properties similar to the bulk material, while particles smaller than *ca.* 20 nm display a drastic increase in the specific heat capacity.[40–42]

To determine the specific heat capacity of the lipid bilayer we consider that the heat capacity of the lipid bilayer-capped UCNPs dispersed in H_2O also comprises a contribution from the lipid bilayer, namely, $m_N c_N = m_p c_p + m_S c_S + m_L c_L$, where m_L and c_L are the mass and specific heat capacity of the lipid bilayer, respectively. Notice that the host $LiYF_4$ was selected because its tetragonal structure yields eight identical {101} faces that all have equal surface energies ($0.82\ J\ m^{-2}$), which promotes a uniform bilayer coverage due to identical host-lipid interactions.[43] The values of the heat capacity of the lipid bilayer are similar when determined using either the calculated photophysical ($715 \pm 57\ J\ kg^{-1}\ K^{-1}$) or the reported ($790\ J\ kg^{-1}\ K^{-1}$)[37–39] c_p values of $LiYF_4$.

Analysis of the transient regime for six laser power densities provided an average value of $5039 \pm 211\ J\ kg^{-1}\ K^{-1}$ ($1.20 \pm 0.06\ cal\ g^{-1}\ K^{-1}$) for the specific heat capacity of the lipid bilayer, which corresponds to a molar heat capacity of $2.93 \pm 0.12\ kJ\ mol^{-1}\ K^{-1}$. This value of the molar heat capacity is similar to those obtained by atomistic molecular dynamics simulations[44] for a dipalmitoylphosphatidylcholine (DPPC) lipid bilayer (Table 2).

Note that the differences in values for the specific heat capacities derive from the significant compositional differences (and hence molecular weight) between our multicomponent bilayer and pure DPPC. Both the current work and the molecular dynamics simulation values are higher than the molar heat capacities measured by differential scanning calorimetry.[45] Even with correction proposed by Blume for lipid phase and chain length, the estimated molar heat capacity of DOPC only increases to $1.98\ kJ\ mol^{-1}\ K^{-1}$. However, molar heat capacities obtained herein are not necessarily directly comparable with the calorimetric results owing not only to significant differences in the composition of the bilayer but also to potential differences in hydrophobic hydration.[45] Notably, prior work has focused on single component ('pure') systems rather than the more biologically relevant and complex, mixed-lipid bilayers studied here.

Conclusions

Using direct measurements of the transient regime under NIR irradiation of an aqueous dispersion of the nanoconstruct comprising upconverting $LiYF_4$:Er^{3+}/Yb^{3+} nanoparticles coated with a conformal lipid bilayer and a power balance model, we demonstrate that the transient regime permits to determine the specific heat capacities of the nanoparticle and the lipid bilayer. The model developed can be considered the first step towards a quantitative description of the dynamics of heat transfer at the nanoscale, which may provide insight into the heat dissipation at the cellular level. The approach described is quite versatile because different solvents can be selected that absorb in the NIR region and which can form stable nanofluids with a diversity of nanoparticles which do not need to be luminescent for this generalized model. Moreover, the model can be used to obtain valuable fundamental biophysical characteristics of different lipid and membrane compositions, such as those in mammalian cells, bacterial cells, and viral lipid envelopes.

Conflicts of interest

There are no conflicts to declare.

Acknowledgements

This work has received funding from the European Union's Horizon 2020 FET Open program under grant agreement no. 801305 and was partially developed in the scope of the projects CICECO-Aveiro Institute of Materials UIDB/50011/2020 & UIDP/50011/2020, financed by Portuguese funds through the FCT/MEC and when appropriate co-financed by FEDER under the PT2020 Partnership Agreement. Financial support from FCT (PTDC/CTM-NAN/4647/2014, NANOHEATCONTROL – POCI-01-0145-FEDER-031469) is acknowledged. J. A. Capobianco is a Concordia University Research Chair in

Nanoscience and is grateful to Concordia University and Natural Science and Engineering Research Council (NSERC) of Canada for the sustained support of his research. C. DeWolf is grateful to NSERC for the support of her research. Ricardo Longo is grateful for the Brazilian Agencies CNPq, CAPES, FACEPE, FINEP, and Pronex for providing partial financial support under grants: Pronex APQ-0675-1.06/14, INCT-NANOMARCS APQ-0549-1.06/17, APQ-1007-1.06/15, and CNPq-PQ fellowship (Proc. 309177/2018-9).

References

1 G. Baffou, H. Rigneault, D. Marguet and L. Jullien, *Nat. Methods*, 2014, **11**, 899–901.
2 S. Kiyonaka, R. Sakaguchi, I. Hamachi, T. Morii, T. Yoshizaki and Y. Mori, *Nat. Methods*, 2015, **12**, 801–802.
3 M. Suzuki, V. Zeeb, S. Arai, K. Oyama and S. Ishiwata, *Nat. Methods*, 2015, **12**, 802–803.
4 M. C. Rajagopal, J. W. Brown, D. Gelda, K. V. Valavala, H. Wang, D. A. Llano, R. Gillette and S. Sinha, *Commun. Biol.*, 2019, **2**, 279.
5 M. Suzuki and T. Plakhotnik, *Biophys. Rev.*, 2020, **12**, 593–600.
6 C. H. Huang and S. S. Li, *Biochim. Biophys. Acta, Rev. Biomembr.*, 1999, **1422**, 273–307.
7 C. Demetzos, *J. Liposome Res.*, 2008, **18**, 159–173.
8 S. Youssefian, N. Rahbar, C. R. Lambert and S. Van Dessel, *J. R. Soc., Interface*, 2017, **14**, 20170127.
9 S. Youssefian, N. Rahbar and S. Van Dessel, *J. Chem. Phys.*, 2018, **148**, 174901.
10 T. Nakano, G. Kikugawa and T. Ohara, *J. Chem. Phys.*, 2010, **133**, 154705.
11 C. D. S. Brites, P. P. Lima, N. J. O. Silva, A. Millán, V. S. Amaral, F. Palacio and L. D. Carlos, *Nanoscale*, 2012, **4**, 4799–4829.
12 D. Jaque and F. Vetrone, *Nanoscale*, 2012, **4**, 4301–4326.
13 B. del Rosal, E. Ximendes, U. Rocha and D. Jaque, *Adv. Opt. Mater.*, 2017, **5**, 1600508.
14 M. Dramićanin, *Luminescence Thermometry: Methods, Materials, and Applications*, Elsevier, Cambridge, 2018.
15 C. D. S. Brites, S. Balabhadra and L. D. Carlos, *Adv. Opt. Mater.*, 2019, **7**, 1801239.
16 T. T. Bai and N. Gu, *Small*, 2016, **12**, 4590–4610.
17 S. Uchiyama, C. Gota, T. Tsuji and N. Inada, *Chem. Commun.*, 2017, **53**, 10976–10992.
18 J. M. Yang, H. Yang and L. W. Lin, *ACS Nano*, 2011, **5**, 5067–5071.
19 L. Shang, F. Stockmar, N. Azadfar and G. U. Nienhaus, *Angew. Chem., Int. Ed.*, 2013, **52**, 11154–11157.
20 A. R. N. Bastos, C. D. S. Brites, P. A. Rojas-Gutierrez, C. DeWolf, R. A. S. Ferreira, J. A. Capobianco and L. D. Carlos, *Adv. Funct. Mater.*, 2019, **29**, 1905474.
21 P. A. Rojas-Gutierrez, C. DeWolf and J. A. Capobianco, *Part. Part. Syst. Charact.*, 2016, **33**, 865–870.
22 R. Hentschke, *Nanoscale Res. Lett.*, 2016, **11**, 88.
23 N. Bogdan, F. Vetrone, G. A. Ozin and J. A. Capobianco, *Nano Lett.*, 2011, **11**, 835–840.
24 J. C. Boyer and F. C. J. M. van Veggel, *Nanoscale*, 2010, **2**, 1417–1419.
25 C. Wurth, M. Kaiser, S. Wilhelm, B. Grauel, T. Hirsch and U. Resch-Genger, *Nanoscale*, 2017, **9**, 4283–4294.
26 S. Balabhadra, M. L. Debasu, C. D. S. Brites, R. A. S. Ferreira and L. D. Carlos, *J. Lumin.*, 2017, **189**, 64–70.
27 C. T. Xu, Q. Q. Zhan, H. C. Liu, G. Somesfalean, J. Qian, S. L. He and S. Andersson-Engels, *Laser Photonics Rev.*, 2013, **7**, 663–697.
28 R. J. Roselli and K. R. Diller, *Biotransport: Principles and Applications*, Springer, New York, 2011.
29 H. A. Michelsen, *J. Chem. Phys.*, 2003, **118**, 7012–7045.
30 H. A. Michelsen, F. Liu, B. F. Kock, H. Bladh, A. Boiarciuc, M. Charwath, T. Dreier, R. Hadef, M. Hofmann, J. Reimann, S. Will, P. E. Bengtsson, H. Bockhorn, F. Foucher, K. P. Geigle, C. Mounaim-Rousselle, C. Schulz, R. Stirn, B. Tribalet and R. Suntz, *Appl. Phys. B: Lasers Opt.*, 2007, **87**, 503–521.
31 T. L. Bergman, A. S. Lavine, F. P. Incropera and D. P. DeWitt, *Fundamentals of Heat and Mass Transfer*, Wiley, New York, 7th edn, 2011.
32 J. Wang, R. R. Deng, M. A. MacDonald, B. L. Chen, J. K. Yuan, F. Wang, D. Z. Chi, T. S. A. Hor, P. Zhang, G. K. Liu, Y. Han and X. Liu, *Nat. Mater.*, 2014, **13**, 157–162.
33 D. W. Lu, C. C. Mao, S. K. Cho, S. Ahn and W. Park, *Sci. Rep.*, 2016, **6**, 18894.
34 R. H. Page, K. I. Schaffers, P. A. Waide, J. B. Tassano, S. A. Payne, W. F. Krupke and W. K. Bischel, *J. Opt. Soc. Am. B*, 1998, **15**, 996–1008.
35 B. SimondiTeisseire, B. Viana, D. Vivien and A. M. Lejus, *Opt. Mater.*, 1996, **6**, 267–274.
36 W. M. Haynes, *CRC Handbook of Chemistry and Physics*, CRC Press, Boca Raton, FL, 2017.
37 S. S. Ballard and J. S. Browder, in *Handbook of Laser Science and Technology*, ed. M. J. Weber, CRC, Boca Raton, FL, 1986, vol. IV, p. 52.
38 L. G. DeShazer and B. A. Wechsler, in *Handbook of Laser Science and Technology*, ed. M. J. Weber, CRC, Boca Raton, FL, 1987, vol. V, p. 328.
39 R. L. Aggarwal, D. J. Ripin, J. R. Ochoa and T. Y. Fan, *J. Appl. Phys.*, 2005, **98**, 103514.
40 M. Saeedian, M. Mahjour-Shafiei, E. Shojaee and M. R. Mohammadizadeh, *J. Comput. Theor. Nanosci.*, 2012, **9**, 616–620.
41 X. M. Wu, L. Wang, Z. C. Tan, G. H. Li and S. S. Qu, *J. Solid State Chem.*, 2001, **156**, 220–224.
42 S. L. Gafner, L. V. Redel, Y. Y. Gafner and V. M. Samsonov, *J. Nanopart. Res.*, 2011, **13**, 6419–6425.
43 P. A. Rojas-Gutierrez, S. Bhuckory, C. Mingoes, N. Hildebrandt, C. DeWolf and J. A. Capobianco, *ACS Appl. Nano Mater.*, 2018, **1**, 5345–5354.
44 L. P. Sun and R. A. Bockmann, *Eur. Biophys. J.*, 2018, **47**, 151–164.
45 A. Blume, *Biochemistry*, 1983, **22**, 5436–5442.

